Investigating the role of deposition on the size distribution of near-surface dust flux during erosion events

Royston Fernandes, Sylvain Dupont, Eric Lamaud

Investigating the role of deposition on the size distribution of near-surface dust flux during erosion events

Royston Fernandes*, Sylvain Dupont, Eric Lamaud

ISPA, INRA, Bordeaux Sciences Agro, F-33140 Villenave d'Ornon, France

Abstract

Predicting the particle-size-distribution (PSD) of near-surface turbulent dust flux (F_{wc}) is a key issue for estimating the size of atmospheric mineral dust. Existing dust emission schemes differ in their parametrization of the emitted dust (F_{emi}) PSD, defining differently the surface inter-particle cohesive force and the influence of wind intensity. Moreover, these schemes have often been validated-fitted against field measurements, assuming PSD similarity between F_{wc} and F_{emi}. Here, we investigate numerically the main factors influencing F_{wc}-PSD during erosion events. To this effect, we developed a 1D dust-dispersal model. After evaluating the model against published results, it is shown that F_{wc}-PSD is influenced by both deposition and F_{emi}-PSD. This latter one is shaped by the inter-particle cohesive bond exponent and the surface dust PSD. A time-to-space conversion of the dust flux variations reveals an increasing enrichment of F_{wc} in small particles compared to F_{emi}. This enrichment remains lower than a few percent of the total dust flux (in number) for fetch lower than 100 m, but it can rise to more than 10% for fetch longer than 1 km. This fetch dependence of F_{wc}-PSD is explained by the slow deposition of particles having the lowest deposition velocities. Importantly, this difference between F_{wc} and F_{emi} PSDs is accentuated with wind intensity, with F_{emi}-PSD dominated by particles with large deposition velocities, and in presence of a large-scale background dust concentration. The role played by the deposition process in shaping the F_{wc}-PSD should be considered when evaluating dust emission schemes against near-surface field measurements.

Keywords: Dust flux, Size distribution, Dust emission, Dust deposition, Deposition velocity

*Corresponding Author
Email address: royston.fernandes@inra.fr (Royston Fernandes)

Investigating the role of deposition on the size distribution of near-surface dust flux during erosion events

Abstract

Predicting the particle size distribution (PSD) of near-surface turbulent dust flux (F_{wc}) is a key issue for estimating the size of atmospheric mineral dust. Existing dust emission schemes differ in their parametrization of the emitted dust (F_{emi}) PSD, defining differently the surface inter-particle cohesive force and the influence of wind intensity. Moreover, these schemes have often been validated-fitted against field measurements, assuming PSD similarity between F_{wc} and F_{emi}. Here, we investigate numerically the main factors influencing F_{wc}-PSD during erosion events. To this effect, we developed a 1D dust-dispersal model. After evaluating the model against published results, it is shown that F_{wc}-PSD is influenced by both deposition and F_{emi}-PSD. This latter one is shaped by the inter-particle cohesive bond exponent and the surface dust PSD. A time-to-space conversion of the dust flux variations reveals an increasing enrichment of F_{wc} in small particles compared to F_{emi}. This enrichment remains lower than a few percent of the total dust flux (in number) for fetch lower than 100 m, but it can rise to more than 10% for fetch longer than 1 km. This fetch dependence of F_{wc}-PSD is explained by the slow deposition of particles having the lowest deposition velocities. Importantly, this difference between F_{wc} and F_{emi} PSDs is accentuated with wind intensity, with F_{emi}-PSD dominated by particles with large deposition velocities, and in presence of a large-scale background dust concentration. The role played by the deposition process in shaping the F_{wc}-PSD should be considered when evaluating dust emission schemes against near-surface field measurements.

Keywords: Dust flux, Size distribution, Dust emission, Dust deposition, Deposition velocity

1. Introduction

Mineral dust aerosols are a fundamental component of the Earth system. They refer to fine suspended soil particles (diameter $< 20\,\mu$m) released by strong winds in regions with erodible soils (Knippertz and Stuut, 2014). The life-cycle of airborne dust involves three stages: (1) the release from the surface, (2) the transport in the atmosphere over long distances by turbulent diffusion and against gravitational sedimentation, and (3) the deposition back on to the surface. These three stages shape the particle size distribution (PSD) of the near-surface dust flux. Interest in understanding the PSD of dust flux is fueled by the impact of the aerosol size on different Earth processes (e.g., Mahowald et al., 2014) such as weather and climate (e.g., Claquin et al., 2003; Otto et al., 2007), ecosystem nutrient supply (e.g., Swap et al., 1992; Knippertz and Stuut, 2014), and human health (e.g., Weuve et al., 2012; Derbyshire, 2007).

The entrainment of dust particles from the surface is driven by sandblasting (e.g., Shao et al., 1993; Marticorena and Bergametti, 1995; Alfaro et al., 1997; Shao and Lu, 2000; Alfaro and Gomes, 2001; Shao, 2001; Kok, 2011b), and, to a lesser extent, by aerodynamic forces (e.g.,

Greeley and Iversen, 1987). Under saltation, dust particles are released when sufficient energy from an impacting saltator is available to break surface inter-particle cohesive bonds (E). In dust emission schemes, saltation is considered as the necessary process for releasing dust. The dust flux is, therefore, often a function of the saltation flux (e.g., Shao et al., 1993; Marticorena and Bergametti, 1995; Alfaro and Gomes, 2001; Shao, 2001; Kok, 2011b; Kok et al., 2014). While the link between saltation and dust fluxes is well established, the processes shaping the PSD of the dust flux remain unclear.

In dust emission schemes, the emitted dust PSD is usually influenced by (1) the surface inter-particle cohesive bond, (2) the soil PSD, and/or (3) the wind intensity, as reviewed below.

The surface inter-particle cohesive bond (E). The parametrization of E differs from one scheme to the other. In Shao et al. (1996), E was assumed proportional to the drag force acting on the particle multiplied by some length scale, leading to $E \propto d_p^3$, where d_p is the diameter of the released dust. Later, Shao (2001) ~~and Kok et al. (2014)~~ related E to the van der Waals bond at the surface, leading to $E \propto d_p^2$. ~~Then Shao (2008) suggested an ensemble surface cohesive bond proportional to the particle size, leading to $E \propto d_p$~~The same was considered by Kok et al. (2014) . Differently, Alfaro and Gomes (2001) proposed an inverse relationship between E and the particle size, $E \propto d_p^{-0.018}$ (deduced from their Table 1). This allowed them to reproduce Alfaro et al. (1997) wind-tunnel experiment where finer particles were released under higher wind conditions, i.e., higher energy of the impacting saltators.

The soil particle size distribution. The influence of the soil PSD on the dust flux changes according to the dust emission schemes. Marticorena and Bergametti (1995) related the dust flux PSD to the percentage of clay present in the soil, i.e., percentage of particles lower than 3.9 μm. In Alfaro and Gomes (2001), the emission of dust is derived from a distribution with three log-normal modes, where the contribution of each mode depends on the strength of the inter-particle cohesive bond and on the wind intensity. In Shao (2001), the emission of dust is derived from ~~a distribution with two modes~~two PSDs, minimally and fully disaggregated ~~modes~~distributions, with an adjustable weight parameter to determine their relative contribution. Kok (2011b) suggested that aggregates behave like brittle materials where the emitted dust PSD is determined by patterns in which cracks nucleate and propagate. A compilation of published flux measurements in Kok et al. (2012) indicated a limited effect of soil texture on the observed dust flux PSD. This insensitivity of the dust flux PSD to the soil granulometry was also suggested in Reid et al. (2008).

The wind intensity. The influence of the wind intensity on the emitted dust PSD remains unclear. On one hand, Shao (2001) and Alfaro and Gomes (2001) considered an enrichment of the dust flux in smaller particles with increasing wind intensity, due to the stronger disintegration of aggregates by adjusting their weight parameters as a function of atmospheric forcing. On the other hand, Kok (2011b) proposed the independence of the emitted dust PSD to the wind intensity, deduced from a compilation of field measurements showing negligible differences of the dust flux PSD under various wind conditions (Kok, 2011a).

The definition of the dust flux simulated by dust emission schemes remained also vague in regard to the measured fluxes used to evaluate-fit them (e.g., Shao et al., 1993; Marticorena and Bergametti, 1995; Shao, 2001; Alfaro and Gomes, 2001; Kok et al., 2014). The dust fluxes simulated by these schemes are ~~most likely the~~ the surface emitted dust fluxes ~~at the surface~~ since these schemes do not explicitly simulate turbulence nor consider the effect of deposition during emission. However, these simulated fluxes have most often been evaluated-fitted against field measurements performed well above the surface (several meters) and at various distances from the upwind border of the dust source area, i.e. fetch sizes ranging from 100 m to

more than 10 km (e.g., Gillette, 1977; Gomes et al., 2003; Gillies and Berkofsky, 2004; Zobeck and Scott Van Pelt, 2006; Fratini et al., 2007; Sow et al., 2009). This implies an hypothesis of PSD similarity between near-surface and surface fluxes, and thus a negligible impact of ~~the~~ both the gravitational settling of the largest particles and the particle surface deposition across all sizes. Only Shao et al. (2011) applied a correction to the measured dust flux to account for the graviational settling but without considering the full deposition process. Dupont et al. (2015) obtained from large-eddy simulations (LES) of aeolian erosion events an increasing difference in PSD with time between near-surface dust flux and emission flux as a result of a first particle sorting through turbulence diffusion, gravitational settling, and more importantly surface deposition. Their results were, however, limited to three particle sizes (1.40, 6.70 and 14.20 μm) and to one soil PSD with an equiprobable emission of the three dust particle sizes, limiting a more general view of the impact of dust deposition on the near-surface dust flux PSD according to the soil PSD. Interestingly, by converting the erosion duration of their simulations into a fetch size, their results mean that the difference in PSD between near-surface dust flux and emission flux should increase with the fetch. A quantification of this difference according to the fetch size and the soil PSD would benefit to the erosion community.

The goal of the present study is twofold: (1) investigate the role of deposition in shaping the PSD of near-surface dust flux during erosion events, and, more generally, (2) investigate the sensitivity of the PSD of near-surface dust flux to the surface inter-particle cohesive bond, the PSD of available dust at the surface, the wind intensity, and the fetch length. To that purpose we extend the initial study of Dupont et al. (2015) by considering (1) dust particles ranging from 0.1 to 16 μm, (2) various soil PSDs, and (3) the influence of the inter-particle cohesive bond exponent (β) on the emitted dust flux PSD. Because the LES approach used in Dupont et al. (2015) was too time consuming for performing such a detailed sensitivity analysis, we developed for this analysis a simple one-dimensional (1D) physically-based dust dispersal model, accounting for dust emission, transport, and deposition in the atmospheric surface boundary layer. After evaluating the model against published dust flux behaviors, the model is used to study the sensitivity of the PSD of the near-surface dust flux.

In this study, the near-surface dust flux will refer to the vertical turbulent-diffusive flux (F_{wc}) at several meters above the surface. It corresponds to the amount of particles transported away from the surface by the flow turbulence. This flux results from a balance between the emission (F_{emi}) and deposition (F_{dep}) fluxes, the storing rate of particles in the air, and the gravitational settling flux (F_{sed}) due to particle weight. Importantly, F_{wc} does not include F_{sed} and it is not equivalent to the dust emission flux at the surface (F_{emi}). See Table 1 for a summary of the flux notations used in this paper.

2. One-dimensional dust-dispersal model

A simple 1D dust-dispersal model was developed to simulate the whole dust life-cycle in a column of air representative of the atmospheric surface boundary layer above an infinite bare erodible surface under neutral thermal stratification (Fig. 1). The model accounts for (1) dust emission through sandblasting, based on an energy budget linking the surface cohesive forces to the dust particle size, (2) dust turbulent transport within the surface boundary layer, and (3) dust deposition at the surface.

2.1. Wind

The wind intensity is quantified through the friction velocity (u_*), which is related to the turbulent flow shear stress (τ) induced by the surface:

$$u_* = \sqrt{\tau/\rho_a}, \tag{1}$$

where ρ_a is the air density. The shear stress quantifies the momentum flux absorbed by the surface. Above an homogeneous surface, τ is constant with height within the surface boundary layer. The similarity theory leads to the well-known logarithmic velocity profile expressed as:

$$u(z) = \frac{u_*}{\kappa} \ln\left(\frac{z}{z_0}\right), \tag{2}$$

where z is the vertical coordinate, z_0 the surface roughness length, and κ the von Karman constant (= 0.40).

In the presence of saltation, the total shear stress (τ) is partitioned within the saltation layer between the momentum flux aborbed by the surface and that absorbed by the saltators. The absorption of momentum by the saltators modifies the wind profile. This was accounted for in Raupach (1991) as:

$$u(z) = \frac{u_*}{\kappa}\left[\ln\left(\frac{z}{z_0}\right) + \left(1 - \sqrt{r}\right)\left[\gamma + \ln\left(\frac{z_0}{H_s}\right) + E\left(\frac{z}{H_s}\right)\right]\right], \tag{3}$$

where $H_s = 0.3969 u_*^2/2g$ is the average height of the saltation layer with g the gravitational acceleration, $r = u_{*,t}^2/u_*^2$ with $u_{*,t}$ the threshold friction velocity above which saltation starts, $\gamma = 0.577216$ is the Eulers constant, and $E(x) = \int_x^\infty \exp(-t)/t dt$. Above the saltation layer, this modification of the wind profile due to saltation is equivalent to replacing z_0 in Equation 2 by a saltation roughness length $z_{0s} = \left[H_s \exp(-\gamma)\right]^{(1-\sqrt{r})} z_0^{\sqrt{r}}$ (Raupach, 1991).

Unlike saltating particles, the relatively small volume fraction of dust particles has negligible effect on the flow field.

2.2. Dust transport

An Eulerian approach was used to describe the turbulent transport of dust particles in the atmospheric surface layer. Here, dust particles were assumed spherical, non magnetic, and electrically neutral. The size range of dust particles is divided into n_b bins, each bin being characterized by a mean particle diameter d_b. Hence, the conservation equation of the dust concentration c_b of the b*th* bin is given by:

$$\frac{\partial c_b(z,t)}{\partial t} = -\frac{\partial F_{wc,b}(z,t)}{\partial z} + v_{s,b}\frac{\partial c_b(z,t)}{\partial z}, \tag{4}$$

where t is time, $F_{wc,b}$ is the dust turbulent-diffusive flux of the b*th* size bin, $v_{s,b}$ is the settling velocity of the particles of the b*th* size bin given as $v_{s,b} = \rho_p g d_b^2 C_c/(18\rho_a \nu)$, where ρ_p is the dust particle density, C_c is the Cunningham slip correction factor, and ν is the kinematic viscosity of air (Seinfeld and Pandis, 1998). Equation 4 means that the dust concentration variation in a grid cell results from a balance between incoming and outgoing turbulent-diffusive ($F_{wc,b}$) and gravitational settling ($F_{sed,b} = v_{s,b}c_b$) fluxes due to turbulent motions and particle weight, respectively.

The turbulent-diffusive dust flux is simply estimated from a flux-gradient relationship:

$$F_{wc,b}(z,t) = -K_d \frac{\partial c_b(z,t)}{\partial z}, \tag{5}$$

where $K_d = \kappa z u_* \left[1 - \left(1 - \sqrt{r}\right) \exp\left(-z/H_s\right)\right]$ is the dust eddy diffusivity assuming similarity in turbulent transport between momentum and dust particles (Gillette et al., 1972). This expression of K_d converges to its surface layer value $\kappa z u_*$ above the saltation layer (Raupach, 1991).

At the surface, the total dust flux (F_{tot}) accounting for both turbulent-diffusive and gravitational settling fluxes, is expressed as:

$$F_{tot,b}^{surf}(t) = F_{emi,b}(t) - F_{dep,b}(t), \tag{6}$$

where $F_{emi,b}$ and $F_{dep,b}$ are the emission and deposition fluxes at the surface of dust particles of the b*th* bin, respectively (Fig. 1).

2.3. Saltation

Saltating particles are characterized by a size distribution p_s whose diameters range from D_{S1} to D_{S2}. The total saltation flux is the integration of the saltation flux of all particle sizes according to p_s:

$$Q_{tot} = \int_{D_{S1}}^{D_{S2}} Q(D) p_s(D) \delta D, \tag{7}$$

where the saltation flux $Q(D)$ of particles of diameter D is estimated from White (1979) as follows:

$$Q(D) = 2.61 \frac{\rho_a}{g} \left(1 + \frac{u_{*,t}(D)}{u_*}\right) \left(1 - \left(\frac{u_{*,t}(D)}{u_*}\right)^2\right) u_*^3, \tag{8}$$

where $u_{*,t}(D)$ is the threshold friction velocity deduced from Marticorena and Bergametti (1995).

On average, the kinetic energy of the saltating particles of diameter D impacting the surface is:

$$E_{imp,D} = \frac{1}{2} m_{imp} v_{imp}^2, \tag{9}$$

where $m_{imp} = \rho_p \pi D^3/6$ is the particle mass, and v_{imp} is the velocity of the impacting saltator. In a first order approximation, v_{imp} is estimated as $v_{imp} = 5u_{*,t}(D)$ (Kok et al., 2014).

Using a probabilistic approach as often used in splash schemes, the kinetic energy of impacting saltators (E_{imp}) is distributed between the energy used for saltator rebound (fraction ϵ_{reb}), the energy used for ejecting new saltators (fraction ϵ_{ej}), and the energy lost to the surface (fraction ϵ_{fr}), such as:

$$\epsilon_{reb} + \epsilon_{ej} + \epsilon_{fr} = 1. \tag{10}$$

Here, $\epsilon_{reb} = 2\gamma^2 P_{reb}$, where P_{reb} is the rebound probability (Anderson and Hallet, 1986) and $\gamma = 0.55$ (Rice et al., 1995); and $\epsilon_{fr} = 0.96\,(1 - \epsilon_{reb})$ (Ammi et al., 2009).

This energy distribution at the surface during the saltator impact does not account for the energy fraction used for releasing dust particles from sandblasting. We hypothesized that the energy for dust emission is a fraction ϵ_d of the energy lost to the surface ($\epsilon_{fr} E_{imp,D}$).

2.4. Dust emission

At the surface, dust particles lie on larger sand grains, surrounded by other dust grains, forming aggregates. A particle in this system experiences short-range dielectric attractive forces known as van der Waals forces due to inter-particle interactions (dust-dust particles or dust-sand particles). Estimating the van der Waals forces between two spherical particles in contact is simple but it becomes much more complex when it comes to estimate the cohesive forces of particles in an aggregate (Shao, 2001). This explains the various parametrizations proposed in the literature for the inter-particle cohesive forces as mentioned in the introduction. Overall, these parametrizations express the inter-particle cohesive bond as a function of the dust particle diameter:

$$E_{coh,b} = A d_b^{\beta}, \tag{11}$$

where β can be referred to as the inter-particle cohesive bond exponent defining the relationship between the dust particle diameter and the cohesive bond, and A is a constant. In existing dust emission schemes, β varies from -0.018 to $+3$ as reviewed in the introduction section.

The number of dust particles of bin b released by an impacting saltator of size D is defined as the ratio between the available energy for releasing dust and the energy required to eject one dust particle:

$$N_{emi,b} = \frac{\epsilon_d \epsilon_{fr} E_{imp,D}}{A d_b^{\beta}}, \tag{12}$$

where ϵ_d is the fraction of the energy lost to the surface by the impacting saltator ($\epsilon_{fr} E_{imp,D}$) that is used to release dust. Equation 12 can be rewritten as:

$$N_{emi,b} = \alpha \frac{\epsilon_{fr} E_{imp,D}}{d_b^{\beta}}, \tag{13}$$

where α is the dust emission coefficient resuming the two unknown constants ϵ_d and A.

Hence, the emission dust flux at the surface of the b*th* bin is:

$$F_{emi,b} = \zeta_d(d_b, u_*) p_d(d_b) \int_{D_{S1}}^{D_{S2}} N_{emi,b}(D) \frac{Q(D)}{l(D)} p_s(D) \delta D, \tag{14}$$

where $p_d(d_b)$ is the proportion of dust particles from the b*th* bin available at the surface, Q/l represents the vertical flux of saltating particles or in other words the flux of impacting saltators at the surface, with l the average hop length of the saltating particles. Here, l was simply deduced as the maximum horizontal distance traveled by a projectile launched with a lift-off velocity V_{ej} and a lift-off angle θ_{ej}: $l = V_{ej}^2 \sin\left(2\theta_{ej}\right)/g$. We chose $V_{ej} = 0.63 u_*$ and $\theta_{ej} = 50°$ (Shao, 2008). The coefficient $\zeta_d(d_b, u_*)$ accounts for the modification of the size distribution of emitted dust due to the enhancement of aggregate disintegration with wind speed as proposed by Alfaro et al. (1997). Unless otherwise specified, $\zeta_d(d_b, u_*) = 1$ in our simulations, implying the size distribution of the emission dust flux is independent of the wind intensity.

2.5. Dust Deposition

Dust deposition on soil occurs only through dry deposition accounting for gravitational settling, turbulent mixing, and brownian diffusion (e.g., Seinfeld and Pandis, 1998). Hence, the deposition flux of dust particles from the bth bin is:

$$F_{dep,b} = v_{dep,b} c_b^{surf}, \tag{15}$$

where c_b^{surf} is the dust concentration close to the surface (middle of the first grid cell, see Fig. 1), and $v_{dep,b}$ is the particle dry deposition velocity that is classically parameterized as a set of resistances:

$$v_{dep,b} = \frac{1}{R_a + R_b + R_a R_b v_{s,b}} + v_{s,b}, \tag{16}$$

where $R_a = \log(z_s/z_{0s}) / (\kappa u_*)$ is the aerodynamic resistance accounting for turbulent transfer near the surface (z_s is the middle of the first grid cell) with z_{0s} the saltation-layer roughness length estimated as per Raupach (1991); $R_b = \left[u_* \left(S_c^{-2/3} + 10^{-3/S_t}\right)\right]^{-1}$ is the quasi-laminar resistance accounting for brownian diffusion and inertial impaction on particles. Here, $S_c = \nu/D_g$ is the Schmidt number, $D_g = k_b T C_c / \left(3\pi\rho_p \nu d_b\right)$ is the brownian diffusivity, with k_b the Boltzman constant, and T the air temperature, set to 27°C in this study. $S_t = u_*^2 v_{s,b} / (g\nu)$ is the Stokes number.

Fig. 2 presents the variation of the deposition velocity with the dust particle size for different wind intensities. The deposition velocity exhibits a minimum for particles around 0.5 to 1 μm in diameter. With increasing wind intensity, the deposition velocity increases, especially for the largest particles, due to the larger decrease of R_b with increasing particle size.

2.6. Simulation configurations

The computational domain was meshed along the vertical using a stretched grid from the surface to the top of the domain. The grid size was varying from $\Delta z_{min} = 0.01$ m at the surface to $\Delta z_{max} = 0.24$ m at the top (Fig. 1). This mesh ensures a grid resolution fine enough to simulate exchanges close to the surface (where particle concentration is high), while reducing the computational time by considering larger grid cells for exchanges farther away. Unless otherwise specified, the total domain height was 200 m corresponding to the approximate depth of the atmospheric surface layer under neutral thermal stratification.

The dust conservation equation (Eq. 4) was solved using the Crank-Nicolson method (Crank and Nicolson, 1947):

$$\frac{c_b^{t+\Delta t} - c_b^t}{\Delta t} = \frac{1}{2}\left[F_i^{t+\Delta t}\left(c_b, z, t+\Delta t, \frac{\partial c_b}{\partial z}, \frac{\partial^2 c_b}{\partial z^2}\right) + F_i^t\left(c_b, z, t, \frac{\partial c_b}{\partial z}, \frac{\partial^2 c_b}{\partial z^2}\right)\right], \tag{17}$$

where $\Delta t = 0.01$ s is the time step and F_i^t is the right-hand side term of Eq. 4 at time t. A Neuman boundary condition was applied at the top of the domain ($\partial c_b/\partial z = 0$). This resolution method has the advantage of being implicit and of ensuring second order convergence in time. The spatial derivatives were discretized following a finite volume approach, ensuring the conservation of the amount of dust particles within the computational domain.

Table 2 summarizes the main input parameters required by our model to simulate dust dispersal during an erosion event. Simulations started with an air clean of dust. Saltating particles had a geometric mean diameter of 210 μm and a geometric standard deviation of 1.8. Dust particle diameters ranged from 0.1 to 16 μm, divided into 15 log-normal bins.

In our simulation analysis, the time variations of dust concentration and dust flux profiles were converted into spatial variations from an upwind virtual border of an erodible surface, corresponding to $t = 0$ s, to distances $x = U_{int}t$, referring to the fetch length, where U_{int} is the integral wind speed ($U_{int} = \int_0^{z_{ref}} u(z)\,dz/z_{ref}$, where z_{ref} was chosen equal to the height of the investigated dust flux, 3 m here, unless otherwise specified). This time-space conversion allows us to evaluate the sensitivity of the dust flux PSD to the deposition process according to the fetch length.

3. Model evaluation

Before using our model to investigate the sensitivity of the near-surface dust flux PSD, we find it important to evaluate its ability to reproduce published dust flux behaviors.

3.1. Dust flux versus wind intensity compared to existing dust emission schemes

Existing dust emission schemes show a clear increase of the dust flux with increasing wind intensity. Here, our model was used to simulate 15-minute erosion events (fetch up to 20 km) with different stationary wind intensities (u_*), starting with an air clean of dust. The surface dust size distribution (p_d) was considered enriched in small particles (D1 distribution in Fig. 3). The cohesive bond exponent β was set to 2. This combination of $\beta = 2$ and distribution D1 leads to an equiprobable PSD of emitted dust. The dust emission coefficient (α) that modulates the amplitude of the dust flux in our model (Eq. 13), was chosen so as the simulated dust flux at $u_* = 0.40\,\mathrm{ms}^{-1}$ fits the one from Shao et al.'s (1993) scheme.

The 3-m high $F_{wc,tot}$, including all particle sizes, as simulated by our model after 15-minute erosion, exhibits a similar trend with u_* as the fluxes obtained from the emission schemes of Shao et al. (1993) and Marticorena and Bergametti (1995) (Fig. 4). This agreement confirms the accurate sensitivity to the wind intensity of the magnitude of the dust flux simulated by our model. The same was verified for different combinations of β and p_d by fitting different values of α.

3.2. Dust concentration vertical profile compared to analytical solution

At steady state over an extended homogenous surface ($F_{emi,b} = F_{dep,b}$), the conservation equation of dust concentration (Eq. 4) leads to the following analytical solution (Shao, 2008):

$$c_b(z) = c_b(z_r)\,(z/z_r)^{v_{s,b}/(\kappa u_*)}\,, \tag{18}$$

where z_r is a reference height.

The concentration profile simulated by our model at equilibrium between $F_{emi,b}$ and $F_{dep,b}$ is consistent with this analytical solution (Fig. 5). This was verified for an erosion event with $u_* = 0.40\,\mathrm{ms}^{-1}$ and 16.0 μm dust particles, in a 35 m high domain. This equilibrium was reached for a fetch $x_{eq} = 36$ km. With a larger domain, x_{eq} increases as the emitted dust particles have a larger volume to disperse, reducing the near-surface dust concentration, and thus the deposition. For typical surface atmospheric boundary layer of 200 m high, $x_{eq} \approx 200$ km. The equilibrium fetch also increases with decreasing particle size. For 5 and 10 μm dust particles and a 200 m high domain, $x_{eq} \approx 320$ and 640 km, respectively. Simulations with particles smaller than 5 μm led to an equilibrium fetch larger than a few thousand kilometers.

3.3. Dust flux enrichment in small particles compared to Dupont et al. (2015) large-eddy simulation

Dupont et al. (2015) performed detailed three-dimensional simulations of soil erosion of a bare surface by representing the main erosion processes (saltation, sandblasting, dust suspension) within a large-eddy simulation (LES) airflow model that simulated instantaneous wind. They simulated 20-minute long erosion events, with three dust particle bins 1.5, 6.7, 14.2 μm, under three wind conditions ($u_* = 0.47, 0.63, 0.77\,\mathrm{ms}^{-1}$). By assuming an equiprobable emission of the three size bins, they observed an enrichment of the 2-m high F_{wc} in small particles with time. This enrichment was explained by the nonstationarity of the erosion process, due to the lower

deposition velocity of the smaller dust particles. Here, we reproduced these simulations with our simple 1D model using similar erosion configurations as in Dupont et al. (2015).

Fig. 6 presents the time variation of the fractions in number of $F_{wc,b}$ on $F_{wc,tot}$, for the three size bins and three wind intensities, as estimated from our model and compared to Dupont et al. (2015). Our 1D model reproduces quite efficiently the flux enrichment in the smallest bin (1.5 μm) and the impoverishment in 6.7 μm particles with time and with increasing wind intensities. The small differences between both models may be explained by the difference in modelling the turbulence in the saltation layer between both approaches.

3.4. Dust flux PSD compared to Alfaro et al. (1997) wind-tunnel experiment

Alfaro et al. (1997) observed from a wind-tunnel experiment an enhancement of the emission of small dust particles with increasing wind intensity. This was observed from the mass size distribution of dust accumulated in a horizontal trap above the surface during a certain period (not specified by the authors). This led them to suggest the enrichment of the emitted dust in small particles with increasing wind intensity and to propose a time-independent dust emission scheme, equivalent to $\beta = -0.018$. Later, Shao (2001) validated his dust emission scheme by reproducing similar time-independent PSD of the dust flux as a function of the wind intensity. To obtain his result, he chose $\beta = 2$ with a different surface dust size distribution than Alfaro et al. (1997).

Here, our 1D model is used to reproduce the Alfaro et al. (1997) experiment by simulating erosion events in a domain with the same vertical size (70 cm) as their wind tunnel. The inter-particle cohesive bond exponent β was set to -0.018 and the surface dust size distribution (Fig. 3) was chosen so as the F_{emi} PSD for $u_* = 0.40\,\mathrm{ms}^{-1}$ equates that observed by Alfaro et al. (1997). Two simulations were conducted: one where F_{emi} PSD exhibited no dependence to the wind intensity ($\zeta(d_b, u_*) = 1$ in Equation 14), and the other one where F_{emi} PSD followed the dependence to the wind intensity proposed by Alfaro et al. (1997) ($\zeta(d_b, u_*) \neq 1$).

Fig. 7 compares the mass size distributions of F_{wc} simulated by the current model and observed by Alfaro et al. (1997), for a 5-m long fetch and three friction velocities. For $u_* = 0.40\,\mathrm{ms}^{-1}$, our model agrees with the observations of Alfaro et al. (1997) regardless of $\zeta(d_b)$. At higher wind speeds, our results only agree with Alfaro et al.'s ones when F_{emi} PSD is a function of the wind speed ($\zeta(d_b, u_*) \neq 1$). This result implies a negligible effect of deposition, sedimentation and turbulence, in shaping the PSD of the near-surface dust flux and, thus, in differentiating the PSDs of F_{wc} and F_{emi}, for the conditions of the wind tunnel experiment. This result leaves open the possibility of the dust flux enrichment in small dust particles with wind intensity due to an enhancement of aggregate disintegration (Alfaro et al., 1997).

3.5. Dust flux PSD compared to Kok (2011b) parametrization

Kok (2011b) proposed a PSD of emitted dust independent of the soil granulometry and wind intensity. They based their proposition on several field data measured at a few meters above the surface and under various fetch magnitudes, ranging from 200 m to 10 km. Here, our model is used to simulate erosion events corresponding to a maximum fetch of 10-km with three wind conditions (u_*), $\beta = 2$, and the surface dust size distribution proposed by Kok (2011b) (Fig. 3). The 3-m high F_{wc} PSD in number simulated by our model (Fig. 8a) is close to that of Kok (2011b) for small fetch lengths (< 5 m). As the fetch increases, the fraction of the largest particles in the dust flux decreases due to their surface deposition, and thus the flux enriches in small particles. This enrichment in small particles (impoverishment in large particles) is accentuated

with u_* as the deposition velocity increases (Fig. 2). The differences between the simulated near-surface dust flux PSD and the emitted flux PSD proposed by Kok (2011b) are amplified when the PSDs are expressed in mass as it emphasizes the role of the largest particles (Fig. 8b).

4. Sensitivity of the dust flux PSD

To investigate the sensitivity of F_{wc} PSD, 10 simulations were conducted varying either (1) the inter-particle cohesive bond exponent (β), (2) the surface dust-size distribution (p_d), or (3) the wind intensity (u_*). Each simulation started from an air clean of dust. This sensitivity of F_{wc} PSD is presented according to the fetch size, with values ranging from 5 m to 10 km. To focus solely on the possible impact of the deposition process on F_{wc} PSD, the F_{emi} PSDs were considered independent of the wind intensity, i.e. $\zeta(d_b, u_*) = 1$ in Equation 14.

Table 3 summarizes the range of each parameter-forcing considered in this analysis. For p_d, four surface dust-size distributions (D1, D2, D3 and D4) were considered (Fig. 3). They were chosen so as to obtain for $\beta = 2$ the following F_{emi} PSDs (Fig. 9d): equinumber emissions across bins (D1), strong emission around 0.7 μm corresponding to particles with the lowest deposition velocity (D2), two emission peaks at 0.7 and 8 μm (D3), and strong emission around 8 μm corresponding to particles with large deposition velocity (D4). Fig. 9 presents the F_{emi} PSDs obtained for the different combinations of β and p_d considered in our analysis. These PSDs cover the usual distributions encountered in existing emission schemes (Alfaro and Gomes, 2001; Shao, 2001; Kok et al., 2014).

The variation of the 3-m high F_{wc} PSDs is presented in number in Fig. 10 according to the fetch size. Fig. 10 includes results for (a) three wind conditions (u_* = 0.30, 0.40 and 0.50 ms^{-1}) with $\beta = 2$ and the surface dust-size distribution D1, (b) three surface dust-size distributions (D2, D3 and D4) with $\beta = 2$ and $u_* = 0.40$ ms^{-1}, and (c) four surface cohesive bond exponents (β = -1,0,1 and 3) with the surface dust-size distribution D1 and $u_* = 0.40$ ms^{-1}. Additionally, Fig. 11 presents the fraction in number and in mass of F_{wc} partitioned in four bins (Z1 to Z4) on the total dust flux $F_{wc,tot}$, according to the fetch size. Here, these four bins cover the whole dust size range. They were defined based on the variations of the particle deposition velocity with the particle size (Fig. 2) such as Z1 bin ($< 0.3\,\mu$m) covers the region of predominant brownian deposition, Z2 bin ($0.3 - 1.0\,\mu$m) covers the region of minimum deposition velocity, Z3 bin ($1.0 - 8.0\,\mu$m) covers the region of sharp rise in deposition velocity, and Z4 bin ($> 8.0\,\mu$m) covers the region of predominant gravitational settling.

An enrichment of F_{wc} in particles with the lowest deposition velocity (Z2 bin) is observed with the fetch when the emitted dust at the surface (F_{emi}) is deprived in dust from the Z2 bin (Fig.10a; D3, D4 in Fig. 10b; $\beta = 0$, 1 in Fig. 10c). This enrichment slightly extents to particles of the Z1 bin (Fig.11a; D3, D4 in Fig. 11b; $\beta = 0$, 1 in Fig. 11c), and implies an impoverishment in particles from Z3 and Z4 bins. When F_{emi} is dominated by particles of the Z2 bin, no enrichment (impoverishment) is observed as F_{emi} is already dominated by particles the least likely to deposit (D2 in Figs. 10b, 11b and $\beta = 3$ in Figs. 10c, 11c).

The resulting difference from this enrichment between F_{wc} and F_{emi} PSDs represents a few percent of the flux for fetch lengths around 100 m, but can rise to about 10% for fetch longer than 1 km (Fig. 11). These percentages are observed for fluxes expressed either in number or in mass. This modification of F_{wc} PSD with the fetch occurs mainly within the first few hundred meters from the upwind border of the source area, then it evolves slowly with the fetch (Fig. 10a). This is visible, for example, in the simulation with the D1 surface PSD and $u_* = 0.50$ ms^{-1} (Fig. 11a)

where the fraction of F_{wc} from bins Z3 and Z4 decreases by nearly 5% within the first 200 m, followed by only a 2% decrease up to 10 km.

The enrichment of F_{wc} in particles of the Z2 bin is accentuated with the wind speed (Figs. 10a and 11a). For a D1 surface PSD and $\beta = 2$, the fraction of F_{wc} from bin Z2 increases by about 2% at a fetch around 100 m between $u_* = 0.30$ and $0.50\,\mathrm{ms}^{-1}$, and by about 5% at fetch longer than 1 km (Fig. 11a). In a different way, for $u_* = 0.50\,\mathrm{ms}^{-1}$, F_{wc} from bin Z2 already reaches in number 39% of the total F_{wc} for a fetch of 100 m while a fetch of 10 km is needed to reach the same fraction for $u_* = 0.30\,\mathrm{ms}^{-1}$ (Fig. 11a). Furthermore, the particle size below which such enrichment occurs decreases from 5 μm to 3 μm (Fig. 10a) when u_* increases from 0.30 to 0.50 ms^{-1}, emphasizing the role of the wind speed in shaping F_{wc} PSD through its impact on the deposition velocity.

The strength of F_{wc} enrichment in small particles depends on the F_{emi} PSD. This latter one is shaped by the combination of the surface PSD and the inter-particle cohesive bond exponent (β) (Fig. 9), β controlling the difference in PSD between the dust available at the surface and the dust emitted from the surface. Regardless of the surface PSD, a high positive value of β (≈ 3) results in a strong emission of the smallest particles, and conversely a strong emission of the largest particles occurs for a small value of β ($\approx$ -1) (Figs. 10c and 11c). The enrichment of F_{wc} in dust of the Z2 bin is minimal for these extreme cases due to either the insignificant concentration of small particles ($\beta \approx$ -1) or the predominant concentration of particles of the Z1-Z2 bins ($\beta \approx 3$) (Fig. 10c).

5. Discussion and conclusion

The particle size distribution (PSD) of the near-surface dust flux (F_{wc}) was found to be mainly influenced by both the deposition process and the size distribution of the emitted dust (F_{emi}).

The F_{emi} PSD appeared shaped from the mutual choice of the size distribution of available dust at the surface (p_d) and the inter-particle cohesive bond exponent (β) (Fig. 9). Different combinations of both quantities can lead to the same F_{emi} PSD. This explains why Shao (2001) and Alfaro and Gomes (2001) were able to reproduce from their schemes the F_{wc} PSD observed by Alfaro et al. (1997) while using different values of β, 2 and -0.018, respectively, and different surface dust size distributions (Fig. 3). Hence, the uncertainty of both quantities in existing dust emission schemes can be simply resolved by defining directly the F_{emi} PSD. Defining F_{emi} PSD becomes, however, all the more complex if p_d is wind speed dependent as suggested by Alfaro et al. (1997).

For constant wind and dust emission conditions, our simulations suggested a distinction between the PSDs of F_{emi} and F_{wc}. This PSD difference increases with the length of the fetch, i.e. the distance from the upwind border of the source area. A difference of a few percent in the flux fraction in number of small dust particles (0.3 to 1 μm) between F_{emi} and F_{wc} PSDs is observed for 100-m long fetch (Fig. 11). This difference can rise to 10% for fetch longer than 1 km. In mass, this difference affects rather larger particles ($> 1\,\mu$m). This modification of F_{emi} and F_{wc} PSDs is explained by the deposition process, as previously found by Dupont et al. (2015) from LES. The deposition of dust particles slowly increases with the fetch as the concentration of dust in the air is enhanced. This process is particle size dependent due to the dependence of the deposition velocity on the particle size (Fig. 2).

Theoretically, the dust deposition should increase with the fetch until an equilibrium is reached between deposition and emission (stationary state). Our simulations showed that this

steady state occurs for fetch lengths larger than a few thousand kilometers for particles lower than 5 μm (section 3.2). This suggests a low probability of reaching a dust steady state during an erosion event. However, this result was obtained for an air clean of dust at the beginning of the simulation, i.e. a clean air upwind from the source area. For a background air already charged in dust particles passing through a source area, the deposition is expected to be larger and the equilibrium between deposition and emission should be reached for smaller fetch lengths. In that configuration of a background dust concentration, the magnitude of the difference in PSD between F_{emi} and F_{wc} should be larger than that observed from our simulations.

Emission and deposition appeared in our simulations as parallel inseparable processes, the impact of the deposition on the F_{wc} PSD being already visible (a few percent) for short fetch around 100 m (Fig. 11). These parallel emission and deposition processes may question the evaluation of existing dust emission schemes. As mentioned in the introduction, these schemes simulate the PSD of emitted dust at the surface (F_{emi}) but have been usually evaluated against measurements performed well above the surface (F_{wc}) where deposition should probably have started to sort particles. Since dust emission schemes do not account for deposition, it was assumed that the PSD of F_{emi} is identical to that of F_{wc}, and time-space independent for stationary wind conditions. Our results suggest that this evaluation procedure is not appropriate when comparing with field experiments, for which fetch lengths usually range from 100 m to several kilometers. However, the small fetch length of wind-tunnel experiments may ensure a PSD similarity between near-surface and surface emitted dust fluxes, as shown in our simulation of the wind-tunnel experiment of Alfaro et al. (1997) (section 3.4).

The wind intensity modifies the F_{wc} PSD by increasing the surface deposition, especially for large particles (Fig. 2), and thereby accelerating the attainment of equilibrium between emission and deposition. A rise of the friction velocity (u_*) from 0.30 to 0.50 ms^{-1} leads to a 10% increase (decrease) of the dust flux fraction of small (large) particles for 1-km long fetch (Fig. 11a). Hence, an observed enrichment of F_{wc} in small particles with wind intensity could be explained by the enhancement of the deposition of larger particles for fetch lengths larger than 100 m, adding to the higher release of small dust through a stronger disintegration of aggregates as proposed by Alfaro et al. (1997).

The magnitude of the difference between F_{emi} and F_{wc} PSDs depends also on the difference in diameter between the particles the most emitted at the surface and the particles with the lowest deposition velocity (around 0.7-2.0 μm following Fig. 2). The farther the peak of F_{emi} PSD is from the minima of the deposition velocity, the greater is the difference in PSDs between F_{wc} and F_{emi} (Fig. 10b,c). Again, this is explained by the dependence of the deposition velocity to the particle size. The near-surface dust flux enriches in particles with the lowest deposition velocity. For F_{emi} dominated by particles with the lowest deposition velocity, the PSDs between F_{emi} and F_{wc} remain similar regardless of the fetch (D2 in Fig. 10b, β=3 in Fig. 10c). This similarity in PSD does not mean an equilibrium between the emission and deposition processes (steady state).

In conclusion, the role of the deposition process when evaluating existing dust emission schemes against field experiments should be considered, especially for large fetch lengths and/or with a large-scale background dust concentration. Improving our prediction of the PSD of F_{wc} requires not only a better understanding of the size distribution of F_{emi} but also a better understanding of the deposition velocity according to the particle size. This is all the more complex as both, emission and deposition processes, are difficult to disentangle in experiments.

References

Alfaro, S.C., Gaudichet, A., Gomes, L., Maillé, M., 1997. Modeling the size distribution of a soil aerosol produced by sandblasting. J. Geophys. Res. 102, 11239–11249.

Alfaro, S.C., Gomes, L., 2001. Modeling mineral aerosol production by wind erosion: Emission intensities and aerosol size distributions in source areas. J. Geophys. Res. 106, 18075–18084.

Ammi, M., Oger, L., Beladjine, D., A, V., 2009. Three-dimensional analysis of the collision process of a bead on a granular packing. Phys. Rev. E. 79, 021305, 1–9.

Anderson, R.S., Hallet, B., 1986. Sediment transport by wind: Toward a general model. GSA Bulletin 97, 523.

Claquin, T., Roelandt, C., Kohfeld, K., Harrison, S., Tegen, I., Prentice, I., Balkanski, Y., Bergametti, G., Hansson, M., Mahowald, N., Rodhe, H., Schulz, M., 2003. Radiative forcing of climate by ice-age atmospheric dust. Clim. Dyn. 20, 193–202.

Crank, J., Nicolson, P., 1947. A practical method for numerical evaluation of solutions of partial differential equations of the heat conduction type, in: Proceedings of the Cambridge Philosophical Society, pp. 50–64.

Derbyshire, E., 2007. Natural minerogenic dust and human health. AMBIO 36, 73–77.

Dupont, S., Alfaro, S.C., Bergametti, G., Marticorena, B., 2015. Near-surface dust flux enrichment in small particles during erosion events. Geophys. Res. Lett. 42, 1992–2000. 2015GL063116.

Fratini, G., Ciccioli, P., Febo, A., Forgione, A., Valentini, R., 2007. Size-segregated fluxes of mineral dust from a desert area of northern china by eddy covariance. Atmos Chem Phys 7, 2839–2854.

Gillette, D., 1977. Fine particulate emissions due to wind erosion. Trans. ASAE 20, 890 – 897.

Gillette, D.A., Blifford Jr., I.H., Fenster, C.R., 1972. Measurements of aerosol size distributions and vertical fluxes of aerosols on land subject to wind erosion. J. Appl. Meteorol. 11, 977–987.

Gillies, J., Berkofsky, L., 2004. Eolian suspension above the saltation layer, the concentration profile. J Sed Res 74, 176–183.

Gomes, L., Rajot, J., Alfaro, S., Gaudichet, A., 2003. Validation of a dust production model from measurements performed in semi-arid agricultural areas of spain and niger. CATENA 52, 257 – 271.

Greeley, R., Iversen, J., 1987. Wind as a Geological Process: On Earth, Mars, Venus and Titan. Cambridge Planetary Science Old, Cambridge University Press.

Knippertz, P., Stuut, J., 2014. Mineral Dust: A Key Player in the Earth System. Springer Netherlands.

Kok, J.F., 2011a. Does the size distribution of mineral dust aerosols depend on the wind speed at emission? Atmos. Chem. Phys. 11, 10149–10156.

Kok, J.F., 2011b. A scaling theory for the size distribution of emitted dust aerosols suggests climate models underestimate the size of the global dust cycle. Proc. Natl. Acad. Sci. 108, 1016–1021.

Kok, J.F., Mahowald, N.M., Fratini, G., Gillies, J.A., Ishizuka, M., Leys, J.F., Mikami, M., Park, M.S., Park, S.U., Van Pelt, R.S., Zobeck, T.M., 2014. An improved dust emission model – part 1: Model description and comparison against measurements. Atmos. Chem. Phys. 14, 13023–13041.

Kok, J.F., Parteli, E.J.R., Michaels, T.I., Bou Karam, D., 2012. The physics of wind-blown sand and dust. Rep. Prog. Phys. 75, 106901.

Mahowald, N., Samuel, A., Kok, J., Engelstaeder, S., Scanza, R., Ward, D.S., Flanner, M.G., 2014. The size distribution of desert dust aerosols and its impact on the earth system. Aeolian Research 15, 53 – 71.

Marticorena, B., Bergametti, G., 1995. Modeling the atmospheric dust cycle: 1. design of a soil-derived dust emission scheme. J. Geophys. Res. Atmos. 100, 16415–16430.

Otto, S., de Reus, M., Trautmann, T., Thomas, A., Wendisch, M., Borrmann, S., 2007. Atmospheric radiative effects of an in situ measured saharan dust plume and the role of large particles. Atmos. Chem. Phys. 7, 4887–4903.

Raupach, M.R., 1991. Saltation layers, vegetation canopies and roughness lengths. Acta Mech. .

Reid, J.S., Reid, E.A., Walker, A., Piketh, S., Cliff, S., Al Mandoos, A., Tsay, S.C., Eck, T.F., 2008. Dynamics of southwest asian dust particle size characteristics with implications for global dust research. J. Geophys. Res. Atmos. 113. D14212.

Rice, M.A., Willets, B.B., McEwan, I.K., 1995. An experimental study of multiple grain-size ejecta produced by collisions of saltating grains with a flat bed. Sedimentology 42, 695–706.

Seinfeld, J., Pandis, S., 1998. Atmospheric chemistry and physics: from air pollution to climate change. A Wiley interscience publication, Wiley.

Shao, Y., 2001. A model for mineral dust emission. J. Geophys. Res. Atmos. 106, 20239–20254.

Shao, Y., 2008. Physics and Modelling of Wind Erosion. Atmospheric and Oceanographic Sciences Library, Springer Netherlands.

Shao, Y., Ishizuka, M., Mikami, M., Leys, J.F., 2011. Parameterization of size-resolved dust emission and validation with measurements. JGR Atm. 116.

Shao, Y., Lu, H., 2000. A simple expression for wind erosion threshold friction velocity. J. Geophys. Res. Atmos. 105, 22437–22443.

Shao, Y., Raupach, M.R., F., L.J., 1996. A model for predicting aeolian sand drift and dust entrainment on scales from paddock to region. Soil Res. 34, 309–342.
Shao, Y., Raupach, M.R., Findlater, P.A., 1993. Effect of saltation bombardment on the entrainment of dust by wind. J. Geophys. Res. Atmos. 98, 12719–12726.
Sow, M., Alfaro, S.C., Rajot, J.L., Marticorena, B., 2009. Size resolved dust emission fluxes measured in niger during 3 dust storms of the amma experiment. Atmos. Chem. Phys. 9, 3881–3891.
Swap, R., Garstang, M., Greco, S., Talbot, R., Kallberg, P., 1992. Saharan dust in the amazon basin. TELLUS B 44, 133–149.
Weuve, J., Puett, R.C., Schwartz, J., Yanosky, J.D., Laden, F., Grodstein, F., 2012. Exposure to particulate air pollution and cognitive decline in older women. Arch. Intern. Med. 172, 219–227.
White, B.R., 1979. Soil transport by winds on mars. J. Geophys. Res. Solid Earth 84, 4643–4651.
Zobeck, T.M., Scott Van Pelt, R., 2006. Wind-induced dust generation and transport mechanics on a bare agricultural field. J. Hazard. Mater 132, 26 – 38.

Flux Nomenclature	
Symbol	**Description**
F_{emi}	Dust emission flux at the surface
F_{dep}	Dust deposition flux at the surface
F_{wc}	Near-surface dust turbulent-diffusive flux
F_{sed}	Dust gravitational settling flux
Indices	
b	Dust particles from the bth bin
tot	All dust particle sizes

Table 1: Dust flux notation.

Parameter	**Symbol**
PSD of available dust at the surface	p_d
PSD of saltating particles	p_s
Dust emission coefficient modulating the number of emitted dust per saltator	α
Inter-particle cohesive bond exponent	β
Function modifying p_d according to the wind intensity	ζ_d
Particle density	ρ_p
Surface roughness length	z_0
Wind friction velocity	u_*
Ambient air properties (temperature, density, kinematic viscosity)	T, ρ_a, ν

Table 2: Main input parameters of our 1D dust dispersal model.

Parameter	**Range of values**
Friction velocity (u_*)	0.30, 0.40, 0.50 ms^{-1}
PSD of available dust at the surface (p_d)	D1, D2, D3, D4 (see, Fig. 3)
Inter-particle cohesive bond exponent (β)	-1, 0, 1, 2, 3

Table 3: Range of values of the parameters considered in our sensitivity analysis of the dust flux PSD.

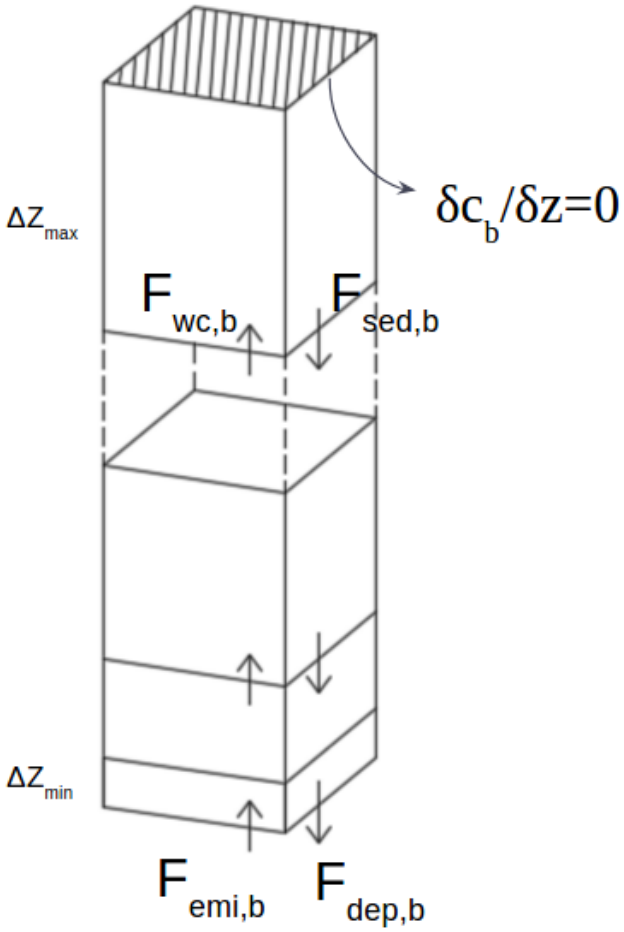

Figure 1: Schematic representation of the 1D computational domain used in this study.

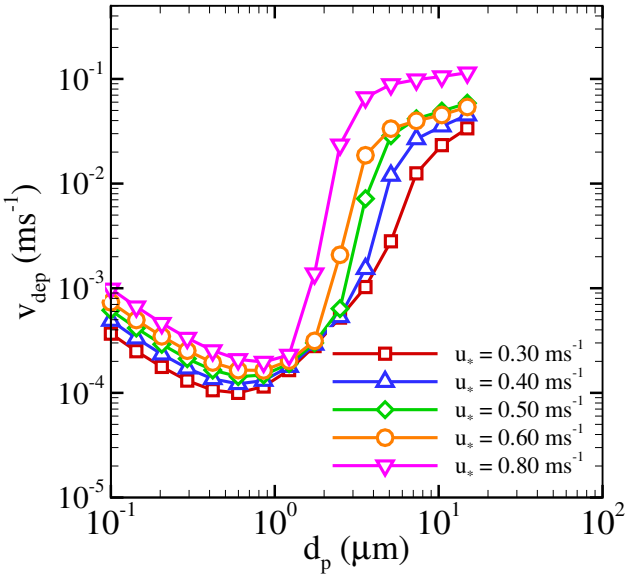

Figure 2: Variation of the deposition velocity (v_{dep}) with dust particle diameter (d_p) for five wind intensities ($u_* = 0.30$, 0.40, 0.50, 0.60 and 0.80 ms^{-1}).

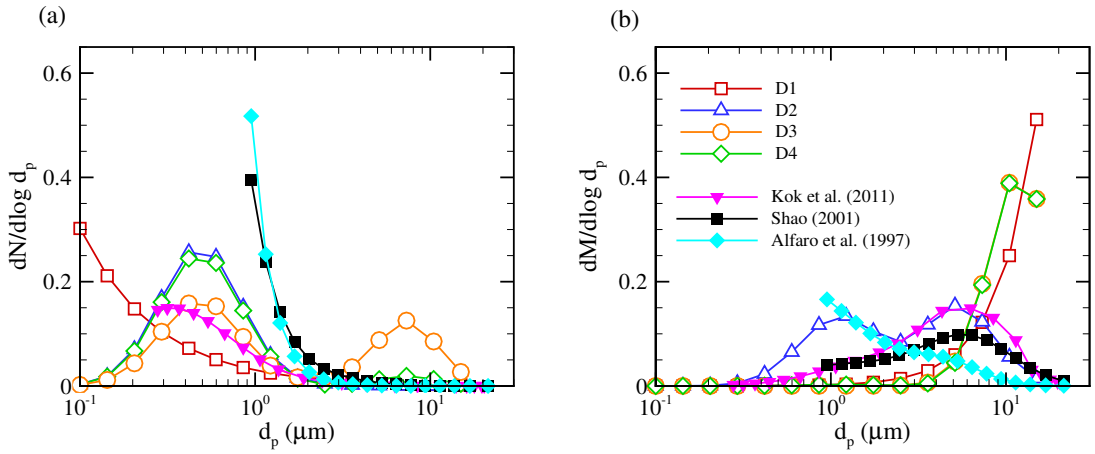

Figure 3: Size distributions in number (a) and in mass (b) of dust particles available at the surface considered in our simulations (D1, D2, D3 and D4) as well as reported in the wind-tunnel experiment of Alfaro et al. (1997) and used in Shao (2001) and Kok (2011a) numerical experiments. The choice of distributions D1 through D4 is explained in section 4.

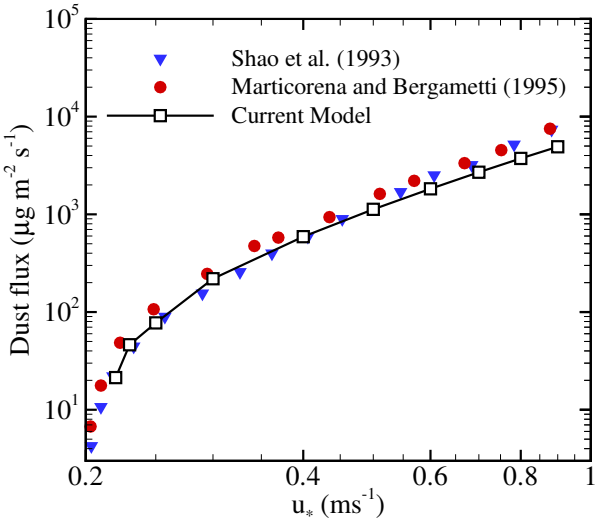

Figure 4: Vertical dust flux ($F_{wc,tot}$), including all particle sizes, as a function of the friction velocity (u_*) obtained from our 1D model and compared with the empirical parametrizations of (1) Marticorena and Bergametti (1995): $F_{wc,tot} = \gamma Q_{tot}$, with $\gamma = 10^{-2}$, and (2) Shao et al. (1993): $F_{wc,tot} = C\rho_d(u_*^2 - u_{*t}^2)$, with $C = 4$ and $u_{*t} = 0.2\,\mathrm{ms}^{-1}$. Note that the dust emission coefficient (α) of our model (Eq. 13) was chosen so as $F_{wc,tot}$ fits the value obtained from Shao et al. (1993) scheme at $u_* = 0.40\,\mathrm{ms}^{-1}$

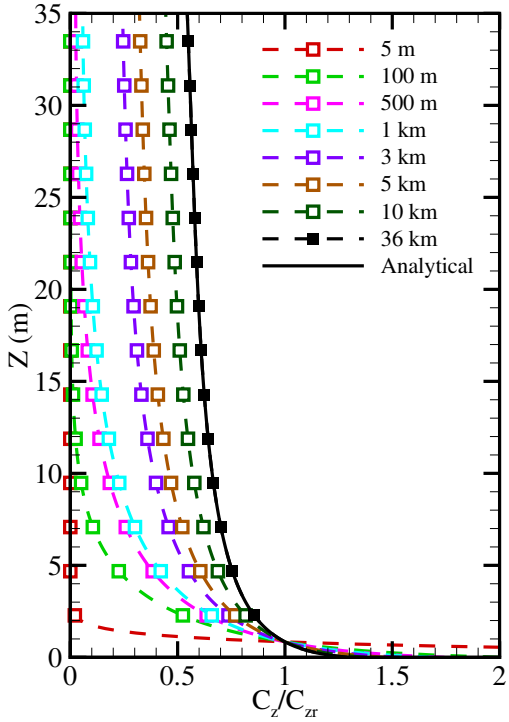

Figure 5: Variation with the fetch length of the simulated vertical dust concentration profiles (dot-lines) and comparison at steady state against the analytical profile (solid line) for 16 μm dust particle in a 35 m high domain, and with $u_* = 0.40\,\mathrm{ms}^{-1}$. The analytical profile responds to $c_b(z) = c_b(z_r)\,(z/z_r)^{v_{s,b}/(\kappa u_*)}$, where z_r is a reference height corresponding here to 1 m.

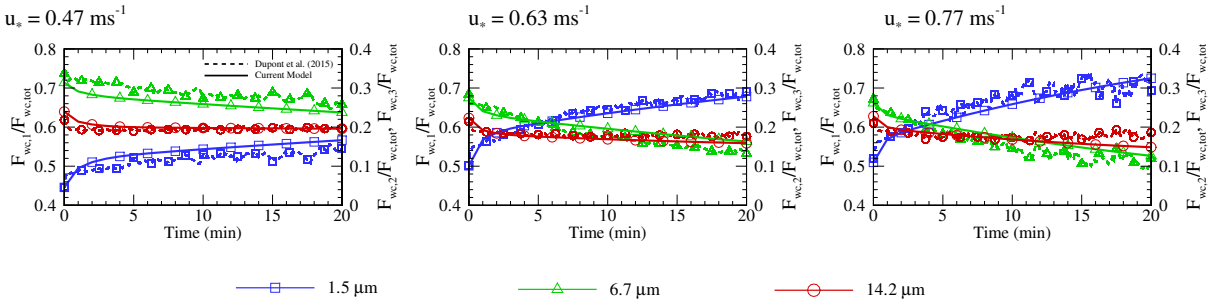

Figure 6: Time variation of the fraction in number of the turbulent-diffusive fluxes ($F_{wc,b}$) at 2 m height of 1.5 μm (blue, b=1), 6.7 μm (green, b=2) and 14.2 μm (red, b=3) particle diameters, on the total turbulent-diffusive dust flux $F_{wc,tot}$, for three wind conditions (u_*) simulated by our model (solid lines) in comparison with those from Dupont et al. (2015) (dotted lines).

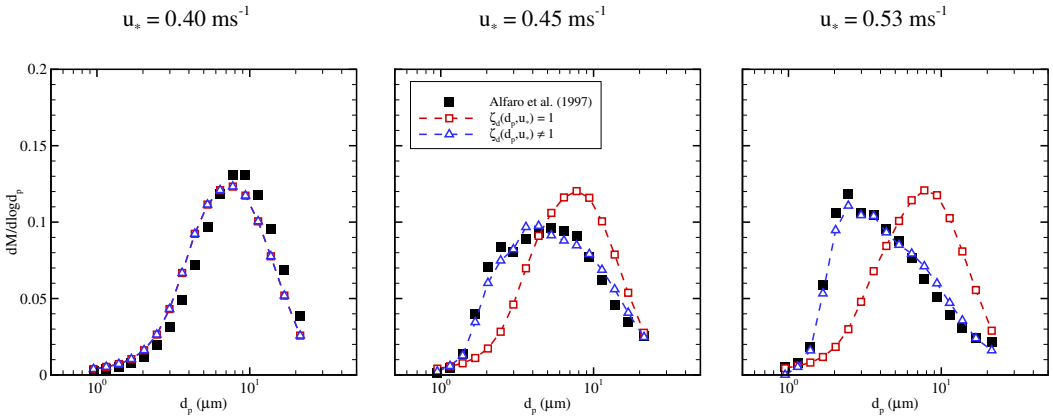

Figure 7: The mass size distribution of the vertical dust fluxes (F_{wc}) as simulated by our model (line-dots) for three wind conditions (u_*), and compared with the wind-tunnel observations from Alfaro et al. (1997) (filled squares). In one simulation, the PSD of available dust at the surface (p_d) is independent of u_* ($\zeta_d = 1$) while in the other simulation p_d depends on u_* as suggested by Alfaro et al. (1997) ($\zeta_d \neq 1$)

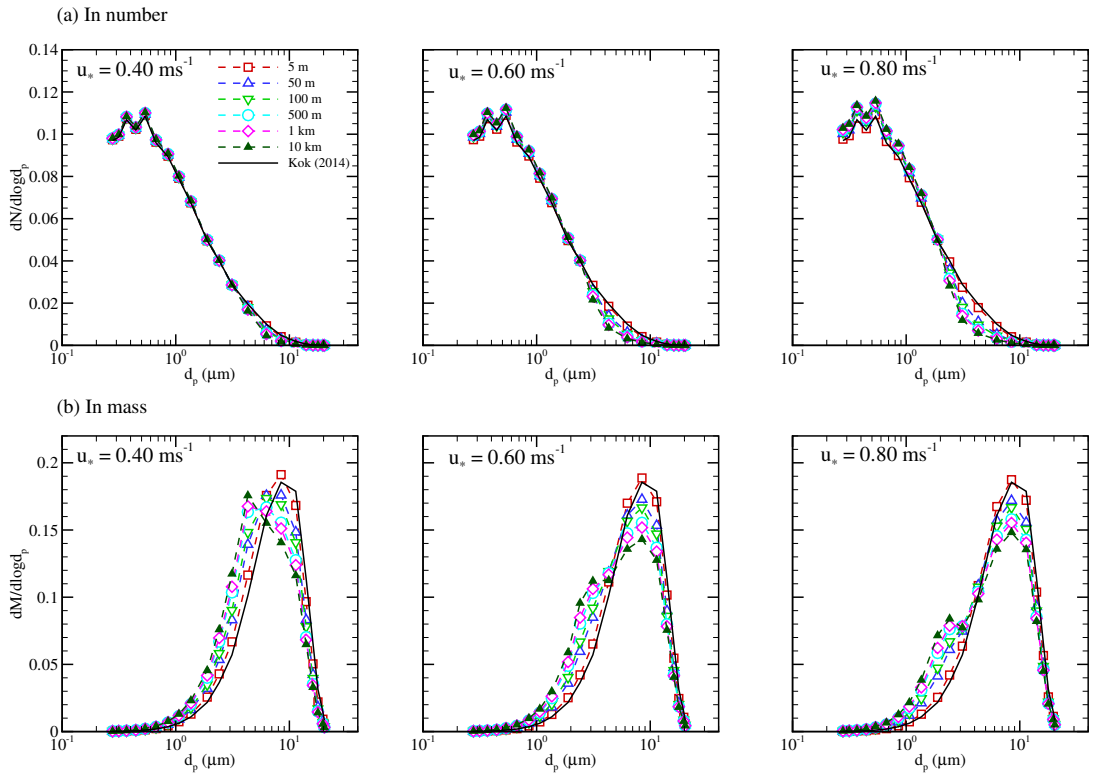

Figure 8: Variation with the fetch length of the size distribution in number (top row) and in mass (bottom row) of the 3-m high vertical dust fluxes (F_{wc}) as simulated by our model (line-dots) for three wind conditions (u_*) (line-dots), and compared with the prediction of Kok (2011b) (solid line-filled squares). The fetch ranges from 5 m to 10 km.

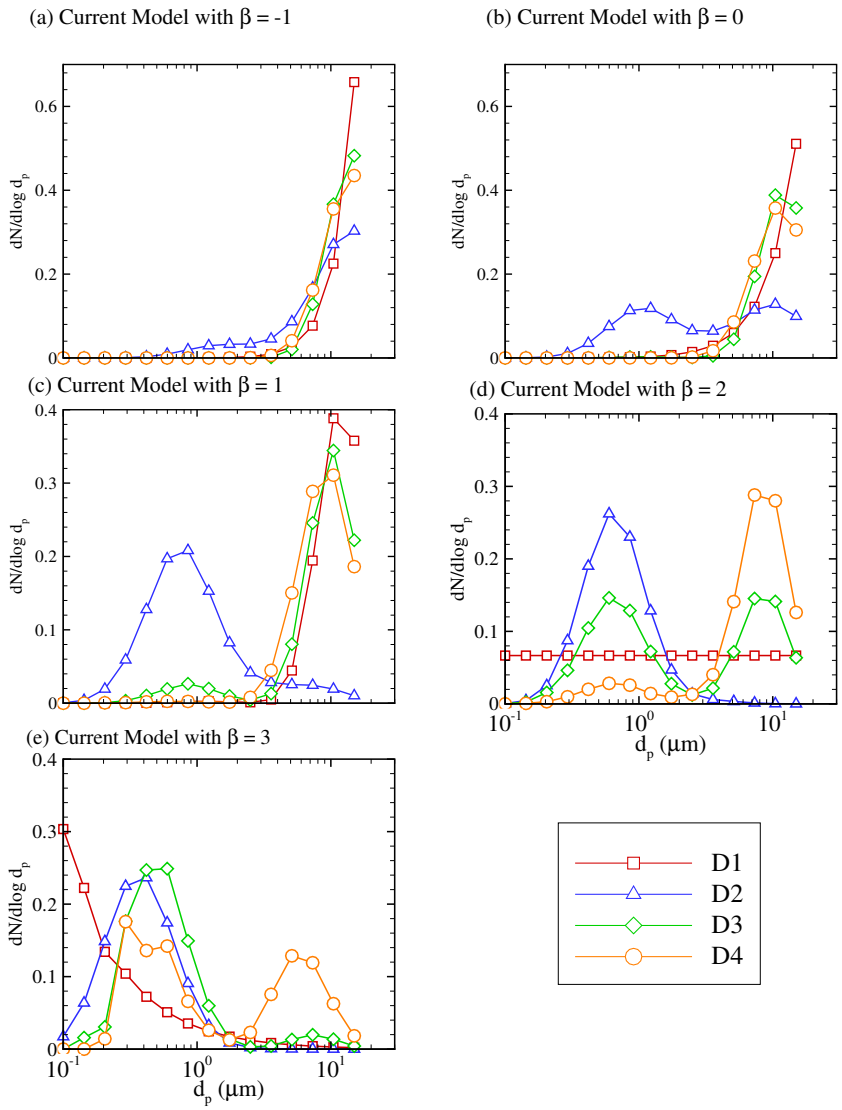

Figure 9: Size distributions in number of emitted dust at the surface (F_{emi}) obtained from our model for various PSD of available dust at the surface (D1, D2, D3 and D4, see Fig. 3) and according to the inter-particle cohesive bond exponent β (from -1 to +3)

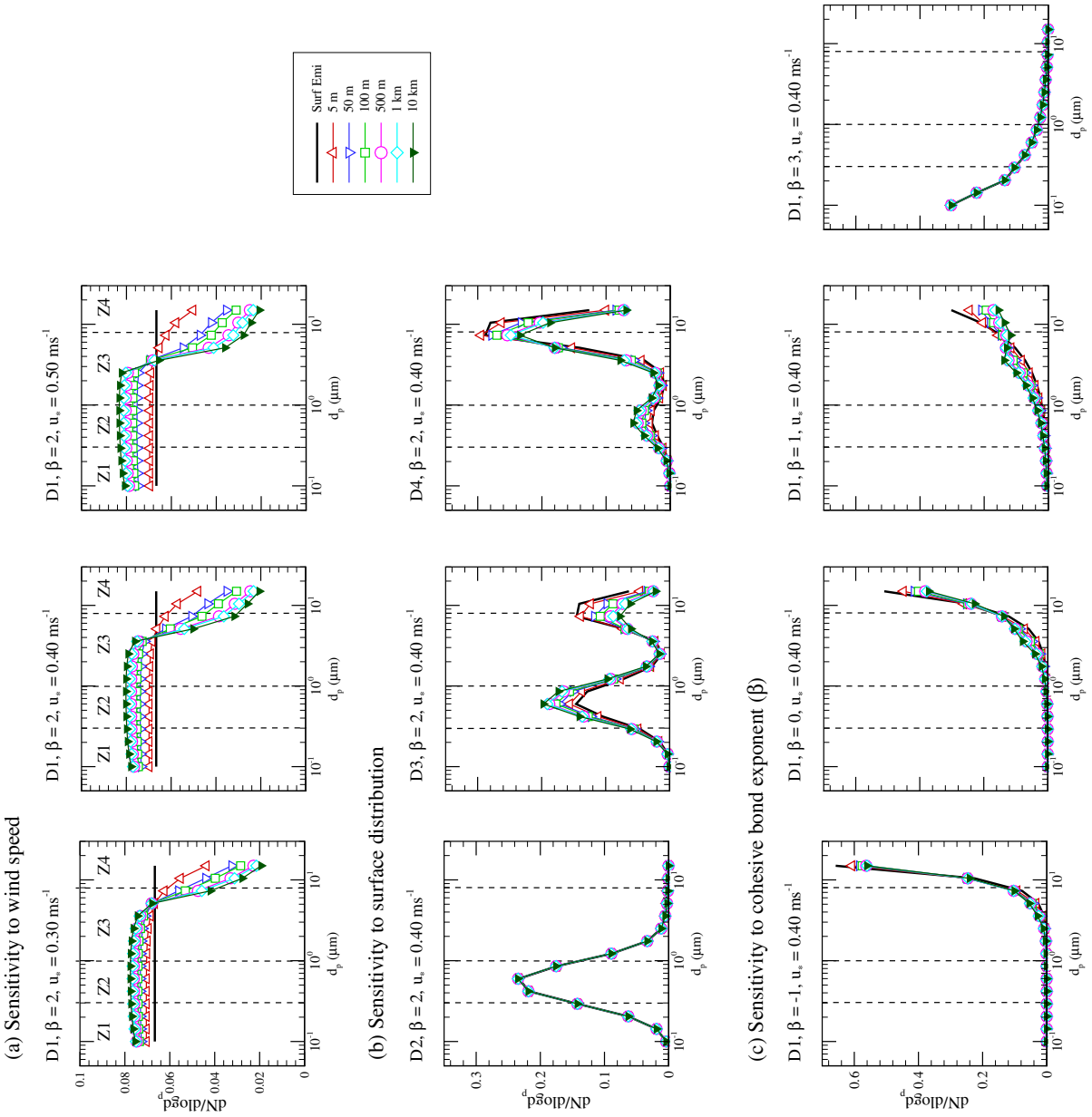

Figure 10: Variation with the fetch length of the size-distribution in number of the 3-m high F_{wc} according to (a) the wind intensity (u_* = 0.30, 0.40 and 0.50 ms^{-1}), (b) the surface dust-size distributions (D2, D3 and D4, see Fig. 3), and (c) the inter-particle cohesive bond exponents (β = -1,0,1 and 3). The fetch ranges from 5 m to 10 km. The dust particle range is divided into 4 bins: Z1 ($d_p \leq$ 0.3 μm) - particles with dominant brownian deposition, Z2 (0.3 μm < $d_p \leq$ 2 μm) - particles the least likely to deposit, Z3 (2 μm < $d_p \leq$ 8 μm) - particles with the deposition velocity the most sensitive to wind intensity, and Z4 ($d_p >$ 8 μm) - particles the most likely to deposit.

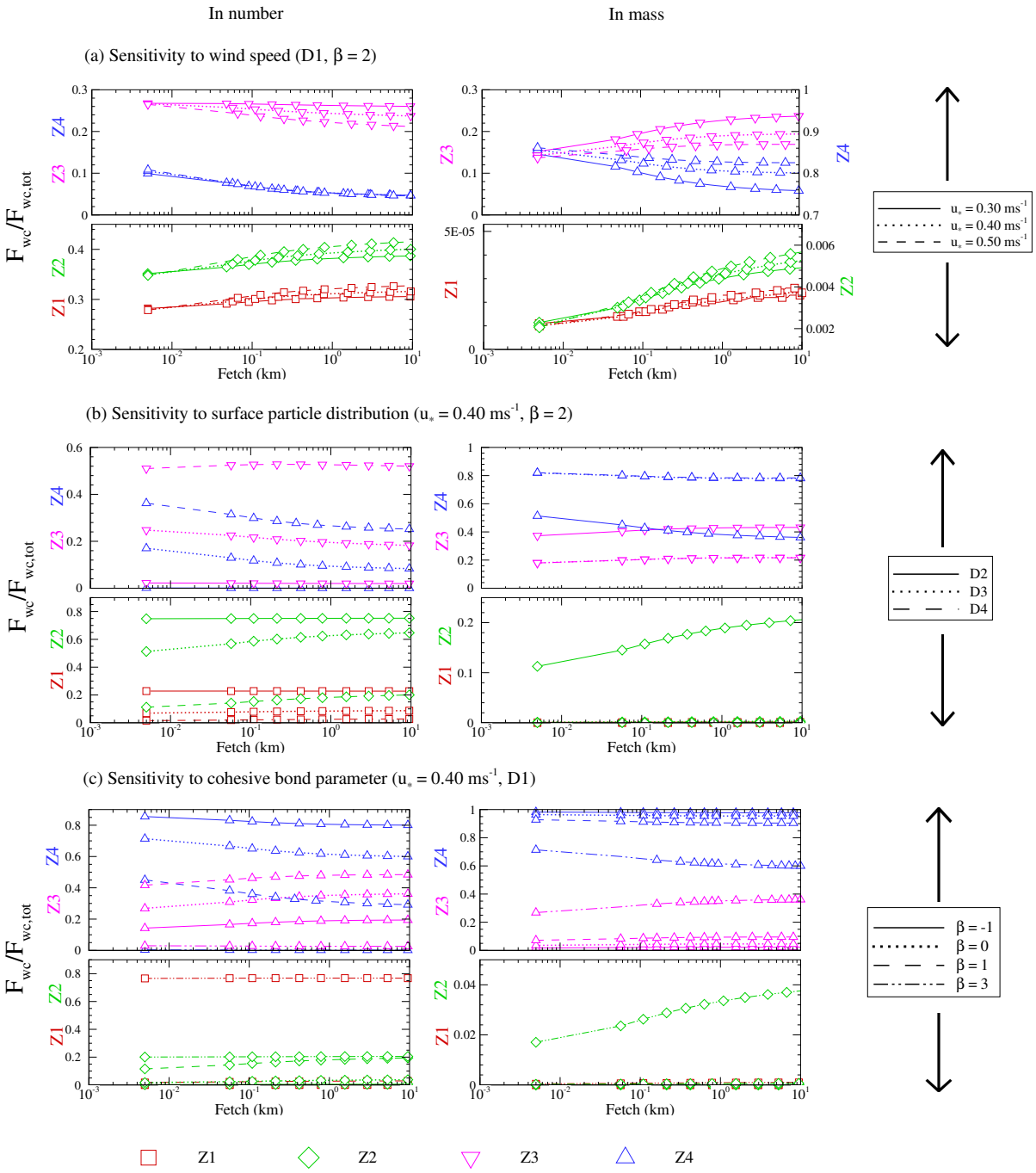

Figure 11: Variation with the fetch length of the fraction in number (left figures) and in mass (right figures) of the 3-m high F_{wc} on the total turbulent-diffusive dust flux $F_{wc,tot}$ according to (a) the wind intensity (u_* = 0.30, 0.40 and 0.50 ms^{-1}), (b) the surface dust-size distributions (D2, D3 and D4, see Fig. 3), and (c) the inter-particle cohesive bond exponents (β = -1,0,1 and 3). F_{wc} is divided into 4 bins: Z1 ($d_p \leq 0.3$ μm) - particles with dominant brownian deposition, Z2 (0.3 μm $< d_p \leq 2$ μm) - particles the least likely to deposit, Z3 (2 μm $< d_p \leq 8$ μm) - particles with the deposition velocity the most sensitive to wind intensity, and Z4 ($d_p > 8$ μm) - particles the most likely to deposit. The fractions at the smallest fetch lengths are equivalent to those of the surface emitted dust flux (F_{emi}).